International Journal of Computer Vision 36(2), 149–161 (2000)

Diffusion of General Data on Non-Flat Manifolds via Harmonic Maps Theory: The Direction Diffusion Case

BEI TANG, GUILLERMO SAPIRO AND VICENT CASELLES
guille@ece.umn.edu

Electrical and Computer Engineering, University of Minnesota, Minneapolis, MN 55455, USA; Escola Superior Politecnica, Universitat Pompeu Fabra, 08002 Barcelona, Spain

Received ; Revised ; Accepted

Abstract. In a number of disciplines, directional data provides a fundamental source of information. A novel framework for isotropic and anisotropic diffusion of directions is presented in this paper. The framework can be applied both to denoise directional data and to obtain multiscale representations of it. The basic idea is to apply and extend results from the theory of harmonic maps, and in particular, harmonic maps in liquid crystals. This theory deals with the regularization of vectorial data, while satisfying the intrinsic unit norm constraint of directional data. We show the corresponding variational and partial differential equations formulations for isotropic diffusion, obtained from an L_2 norm, and edge preserving diffusion, obtained from an L_p norm in general and an L_1 norm in particular. In contrast with previous approaches, the framework is valid for directions in any dimensions, supports non-smooth data, and gives both isotropic and anisotropic formulations. In addition, the framework of harmonic maps here described can be used to diffuse and analyze general image data defined on general non-flat manifolds, that is, functions between two general manifolds. We present a number of theoretical results, open questions, and examples for gradient vectors, optical flow, and color images.

Keywords: directions, isotropic and anisotropic diffusion, multiscale representations, harmonic maps, general non-flat manifolds, liquid crystals, gradients, optical flow, color images

1. Introduction

In a number of disciplines, directions provide a fundamental source of information. Examples in the area of computer vision are (2D, 3D, and 4D) gradient directions, optical flow directions, surface normals, principal directions, and color. In the color example, the direction is given by the normalized vector in the color space. Frequently, this data is available in a noisy fashion, and there is a need for noise removal. In addition, it is often desired to obtain a multiscale-type representation of the directional data, similar to those representations obtained for gray-level images (Koenderink, 1984; Perona, 1998; Perona and Malik, 1990; Witkin, 1993). Addressing these issues is the goal of this paper.

Image data, as well as directions and other sources of information, are not always defined on the $\mathbb{R}^2$ plane or $\mathbb{R}^3$ space. They can be, for example, defined over a surface embedded in $\mathbb{R}^3$. It is also important then to extend the scale space and diffusion frameworks to general data, defined on general (not-necessarily flat) manifolds. In other words, we want to deal with maps between two general manifolds, and be able to isotropically and anisotropically diffuse them. This will make it possible for example to denoise data defined on 3D surfaces. Although we are particularly interested in this paper in directions defined on $\mathbb{R}^2$ (non-flat data

defined on a flat manifold), the framework here presented applies to the general case as well.

An $\mathbb{R}^n$ direction defined on an image in $\mathbb{R}^2$ is given by a vector $I(x, y, 0) : \mathbb{R}^2 \to \mathbb{R}^n$ such that the Euclidean norm of $I(x, y, 0)$ is equal to one, that is,

$$\sqrt{\sum_{i=1}^{n} I_i^2(x, y, 0)} = 1,$$

where $I_i(x, y, 0) : \mathbb{R}^2 \to \mathbb{R}$ are the components of the vector. The notation can be simplified by considering $I(x, y, 0) : \mathbb{R}^2 \to S^{n-1}$, where S^{n-1} is the unit ball in $\mathbb{R}^n$. This implicitly includes the unit norm constraint. (Any non-zero vector can be transformed into a direction by normalizing it. For zero vectors, the unit norm constraint has to be relaxed, and a norm less or equal to one needs to be required.) When smoothing the data, or computing a multiscale representation $I(x, y, t)$ of a direction $I(x, y, 0)$ (t stands for the scale), it is crucial to maintain the unit norm constraint, which is an intrinsic characteristic of directional data.[1] That is, the smoothed direction $\hat{I}(x, y, 0) : \mathbb{R}^2 \to \mathbb{R}^n$ must also satisfy

$$\sqrt{\sum_{i=1}^{n} \hat{I}_i^2(x, y, 0)} = 1.$$

Or, $\hat{I}(x, y, 0) : \mathbb{R}^2 \to S^{n-1}$. The same constraint holds for a multiscale representation $I(x, y, t)$ of the original direction $I(x, y, 0)$. This is what makes the smoothing of directions different from the smoothing of ordinary vectorial data as in Blomgren and Chen (1998), Sapiro and Ringach (1996), Sochen et al. (1998), Weickert (1997), Whitaker and Gerig (1994), Yezzi (1998): The smoothing is performed in S^{n-1} instead of $\mathbb{R}^n$.

Directions can also be represented by the angle(s) the vector makes with a given coordinate system, denoted in this paper as *orientation*(s). In the 2D case for example, the direction of a vector (I_1, I_2) can be given by the angle θ that this vector makes with the x axis (we consider $\theta \in [0, 2\pi)$): $\theta = \arctan(I_2/I_1)$ (with the corresponding sign considerations to have the map in the $[0, 2\pi)$ interval). There is of course a one-to-one map between a direction vector $I(x, y) : \mathbb{R}^2 \to S^1$ and the angle function $\theta(x, y)$. Using this relation, Perona (1998), well motivated the necessity for orientation and direction diffusion and transformed the problem of 2D direction diffusion into a 1D problem of angle or orientation diffusion (see additional comments in Section 3 below). Perona then proposed PDE's based techniques for the isotropic smoothing of 2D orientations; see also Granlund and Knutsson (1995) and Weickert (1996) and the general discussion of these methods in Perona (1998). Smoothing orientations instead of directions solves the unit norm constraint, but adds a periodicity constraint. Perona showed that a simple heat flow (Laplacian or Gaussian filtering) applied to the $\theta(x, y)$ image, together with special numerical attention, can address this periodicity issue. Unfortunately, this pioneering approach is not rotational invariant, and theoretically it applies only to smooth data (indeed to vectors with coordinates in the Sobolev space $W^{1,2}$), and thereby disqualifying edges. The straightforward extension of this to S^{n-1} would be to consider $n - 1$ angles, and smooth each one of these as a scalar image. The natural coupling is then missing, obtaining a set of decoupled PDE's. Additional comments on this orientation diffusion technique will be given when presenting our approach.

Remark. As Perona pointed out in his work, directional data is just one example of the diffusion of images representing data beyond flat manifolds. Extensions to Perona's work, using intrinsic metrics on the manifold can be found in Chan and Shen (1999) and Sochen et al. (1998). In Chan and Shen (1999) (this work was performed simultaneously and independently to ours), the authors explicitly deal with orientations (no directions) and present the L_1 norm as well as many additional new features, contributions on discrete formulations, and connections with our approach. The work (Sochen et al., 1998) does not deal with orientations or directions. In Rudin and Osher (1994) the authors also mention the minimization of the L_1 norm of the divergence of the normalized image gradient (curvature of the level-sets). This is done in the framework of image denoising, without addressing the regularization and analysis of directional data or presenting examples. None of these works explicitly uses or mentions the classical and "natural" harmonic maps framework as we do in this paper. Note that not only the data (e.g., directions) can go beyond flat manifolds, but its domain can also be non-flat (e.g., the data can be defined on a surface). The harmonic framework here described addresses the non-flatness of both manifolds. That is, with the general framework here introduced we can obtain isotropic and anisotropic diffusion and scale-spaces for any function mapping two manifolds (see also Sochen et al. (1998), a framework also permitting this). We can for example diffuse (and denoise) data on a 3D surface, or diffuse posterior probability vectors

(Pardo and Sapiro, 1999). In this paper we present the general framework and detail the case of directions defined on the plane, while other cases are described elsewhere.

In this work we follow the suggestion in Caselles and Sapiro (1998) and directly perform diffusion on the direction space, extending to images representing directions the by now already classical results on diffusion of images representing gray values (Alvarez et al., 1992; Koenderink, 1984; Perona and Malik, 1990; Rudin et al., 1992; Sapiro and Ringach, 1996; Weickert, 1996; Whitaker and Gerig, 1994). That is, from the original unit norm vectorial image $I(x, y, 0) : \mathbb{R}^2 \to S^{n-1}$ we construct a family of unit norm vectorial images $I(x, y, t) : \mathbb{R}^2 \times [0, \tau) \to S^{n-1}$ that provides a multiscale representation of directions. The method intrinsically takes care of the normalization constraint, eliminating the need to consider orientations and develop special periodicity preserving numerical approximations. Discontinuities in the directions are also allowed by the algorithm. The approach follows results from the literature on harmonic maps in liquid crystals, and $I(x, y, t)$ is obtained from a system of coupled partial differential equations that reduces a given (harmonic) energy. Energies giving both isotropic and anisotropic flows will be described. Due to the large amount of literature in the subject of harmonic maps applied to liquid crystals, a number of relevant theoretical results can immediately be obtained.

Before presenting the details of the framework for direction diffusion here proposed, let's resume its main unique characteristics:

1. It includes both isotropic and anisotropic diffusion.
2. It works for directions in any dimension.
3. It supports non-smooth data.
4. The general framework includes also directions and general image data defined on general manifolds, e.g., surface normals, principal directions, and images on 3D surfaces.
5. It is based on a substantial amount of existing theoretical results that help to answer a number of relevant computer vision questions.

2. The General Problem

Let $I(x, y, 0) : \mathbb{R}^2 \to S^{n-1}$ be the original image of directions. That is, this is a collection of vectors from $\mathbb{R}^2$ to $\mathbb{R}^n$ such that their unit norm is equal to one, i.e., $\|I(x, y, 0)\| = 1$, where $\|\cdot\|$ indicates Euclidean length. $I_i(x, y, 0) : \mathbb{R}^2 \to \mathbb{R}$ stand for each one of the n components of $I(x, y, 0)$. We search for a family of images, a multiscale representation, of the form $I(x, y, t) : \mathbb{R}^2 \times [0, \tau) \to S^{n-1}$, and once again we use $I_i(x, y, t) : \mathbb{R}^2 \to \mathbb{R}$ to represent each one of the components of this family. Let us define the *component gradient* ∇I_i as

$$\nabla I_i := \frac{\partial I_i}{\partial x}\vec{x} + \frac{\partial I_i}{\partial y}\vec{y}, \tag{1}$$

where $\vec{x}$ and $\vec{y}$ are the unit vectors in the x and y directions respectively. From this,

$$\|\nabla I_i\| = \left(\left(\frac{\partial I_i}{\partial x}\right)^2 + \left(\frac{\partial I_i}{\partial y}\right)^2\right)^{1/2}, \tag{2}$$

gives the absolute value of the component gradient.

The *component Laplacian* is given by

$$\Delta I_i = \frac{\partial^2 I_i}{\partial x^2} + \frac{\partial^2 I_i}{\partial y^2}. \tag{3}$$

We are also interested in the *absolute value of the image gradient*, given by

$$\|\nabla I\| := \left(\sum_{i=1}^{n}\left(\left(\frac{\partial I_i}{\partial x}\right)^2 + \left(\frac{\partial I_i}{\partial y}\right)^2\right)\right)^{1/2}. \tag{4}$$

Having this notation, we are now ready to formulate our framework. The problem of *harmonic maps in liquid crystals* is formulated as the search for the solution to

$$\min_{I:\mathbb{R}^2 \to S^{n-1}} \int\int_{\Omega} \|\nabla I\|^p \, dx \, dy, \tag{5}$$

where Ω stands for the image domain and $p \geq 1$. This variational formulation can be re-written as

$$\min_{I:\mathbb{R}^2 \to \mathbb{R}^n} \int\int_{\Omega} \|\nabla I\|^p \, dx \, dy, \tag{6}$$

such that

$$\|I\| = 1. \tag{7}$$

This is a particular case of the search for maps I between Riemannian manifolds (M, g) and (N, h) which are critical points (that is, minimizers) of the *harmonic energy*

$$E_p(I) = \int_M \|\nabla_M I\|^p \mathrm{dvol}M, \tag{8}$$

where $\|\nabla_M I\|$ is the length of the differential in M. In our particular case, M is a domain in $\mathbb{R}^2$ and $N = S^{n-1}$, and $\|\nabla_M I\|$ reduces to (4). The critical points of (8) are called *p-harmonic maps* (or simply *harmonic maps* for $p = 2$). This is in analogy to the critical points of the Dirichlet energy $\int_\Omega \|\nabla f\|^2$ for real valued functions f, which are called *harmonic functions*.

The general form of the harmonic energy, normally from a 3D surface (M) to the plane (N) with $p = 2$ (the most classical case, e.g., Eells and Lemarie (1978, 1988)), was successfully used for example in computer graphics to find smooth maps between two given (triangulated) surfaces (again, normally a surface and the complex or real plane); e.g. Eck et al. (1995), Angenent et al. (1998), Haker et al. (1999) and Zhang and Hebert (1999). In this case, the search is indeed for the critical point, that is, for the harmonic map between the surfaces. This can be done for example via finite elements (Angenent et al., 1998, Haker et al. (1999). In our case, the problem is different. We already have a candidate map, the original (normally noisy or with many details at all scales) image of directions $I(x, y, 0)$, and we want to compute a multiscale representation or regularized/denoised version of it. That is, we are not (just) interested in the harmonic map between the domain in $\mathbb{R}^2$ and S^{n-1} (the critical point of the energy), but are interested in the process of computing this map via partial differential equations. More specifically, we are interested in the gradient-descent type flow of the harmonic energy (8). This is partially motivated by the fact that the basic diffusion equations for multiscale representations and denoising of gray-valued images are obtained as well as gradient descent flows acting on real-valued data; see for example Black et al. (1998), Perona and Malik (1990), Rudin et al. (1992) and You et al. (1996). Isotropic diffusion (linear heat flow) is just the gradient descent of the L_2 norm of the image gradient, while anisotropic diffusion can be interpreted as the gradient descent flow of more robust functions acting on the image gradient.

Since we have an energy formulation, it is straightforward to add additional data-dependent constraints on the minimization process, e.g., preservation of the original average; see for example Rudin et al. (1992) for examples for gray-valued images. In this case we might indeed be interested in the critical point of the modified energy, which can be obtained as the steady-state solution of the corresponding gradient descent flow.[2]

For the most popular case of $p = 2$, the Euler-Lagrange equation corresponding to (8) is a simple formula based on Δ_M, the Laplace-Beltrami operator of M, and $A_N(I)$, the second fundamental form of N (assumed to be embedded in $\mathbb{R}^k$) evaluated at I; e.g., Eells and Lemarie (1978, 1988) and Struwe (1985):

$$\Delta_M I + A_N(I)\langle \nabla_M I, \nabla_M I\rangle = 0. \tag{9}$$

This leads to a gradient-descent type of flow, that is,

$$\frac{\partial I}{\partial t} = \Delta_M I + A_N(I)\langle \nabla_M I, \nabla_M I\rangle. \tag{10}$$

In the following sections, we will present the gradient descent flows for our particular energy (5), that is, for M being a domain in $\mathbb{R}^2$ and N equal to S^{n-1}.[3] We concentrate on the cases of $p = 2$, isotropic, and $p = 1$, anisotropic (or in general $1 \le p < 2$). The use of $p = 2$ corresponds to the classical heat flow from the linear scale-space theory (Koenderink, 1984; Witkin, 1993), while the case $p = 1$ corresponds to the *total variation* flow studied in Rudin et al. (1992).

Most of the literature on harmonic maps deals with $p = 2$ in (8) or (5), the linear case. Some more recent results are available for $1 < p < \infty$, $p \neq 2$, (Chen et al., 1994; Coron and Gulliver, 1989), and very few results deal with the case $p = 1$ (Giaquinta et al., 1993). A number of theoretical results, both for the variational formulation and its corresponding gradient descent flow, which are relevant to the multiscale representation of directions, will be given in the following sections as well. The papers (Eells and Lemarie, 1978, 1988) are an excellent source of information for regular harmonic maps, while (Hardt, 1997) contains a comprehensive review of singularities of harmonic maps (check also Struwe (1985), a classic on harmonic maps). A classical paper for harmonic maps in liquid crystals, that is, the particular case of (5) (or in general, M being a domain in $\mathbb{R}^n$ and $N = S^{n-1}$), is Brezis et al. (1986).

3. Isotropic Diffusion

It is easy to show, see Appendix,[4] that for $p = 2$, the gradient descent flow corresponding to (6) with the constraint (7) is given by the set of coupled PDE's:

$$\frac{\partial I_i}{\partial t} = \Delta I_i + I_i \|\nabla I\|^2, \quad 1 \le i \le n. \tag{11}$$

This system of coupled PDE's defines the isotropic multiscale representation of $I(x, y, 0)$, which is used as initial data to solve (11). (Boundary conditions are also added in the case of finite domains.)

The first part of (11) comes from the variational form, while the second one comes from the constraint (see for example Struwe (1990)). As expected, the first part is decoupled between components I_i, and linear, while the coupling and non-linearity come from the constraint.

If $n = 2$, that is, we have 2D directions, then it is easy to show that for (smooth data) $I(x, y) = (\cos\theta(x, y), \sin\theta(x, y))$, the energy in (5) becomes $E_p(\theta) := \int\int_\Omega (\theta_x^2 + \theta_y^2)^{p/2}\, dx\, dy$. For $p = 2$ we then obtain the linear heat flow on θ ($\theta_t = \Delta\theta$) as the corresponding gradient descent flow, as expected from the results in Perona (1998). The precise equivalence between the formulation of the energy in terms of directions, $E_p(I)$, and the formulation in terms of orientations, $E_p(\theta)$, is only true for $p \geq 2$ (Bethuel and Zheng, 1988; Giaquinta et al., 1993). In spite of this connection, and as was pointed out in Giaquinta et al. (1993), using directions and orientations is not fully equivalent. Observe for example the map $v(X) = \frac{X}{\|X\|}$ defined on the unit ball B^2 of $\mathbb{R}^2$. On one hand, this map has finite E_p energy if, and only if, $1 \leq p < 2$. On the other hand, the map cannot be defined with an angle function $\theta(x, y)$, θ being in the Sobolev space $W^{1,p}(B^2)$. As pointed out in Giaquinta et al. (1993), the only obstruction to this representation is the index of the vector of directions. Thus, smooth directions can lead to non-smooth orientations (Perona's goal in the periodic formulations he proposes is in part to address this issue). This problem then gives an additional advantage to selecting a directions-based representation instead of an orientations one.

For the isotropic case, $p = 2$, we have the following important results from the literature on harmonic maps:

Existence: Existence results for harmonic mappings were already reported in Eells and Sampson (1964) for a particular selection of the target manifold N (non-positive curvature). Struwe (1985) showed, in one of the classical papers in the area, that for initial data with finite energy (as measured by (8)), M a two dimensional manifold with $\partial M = \emptyset$ (manifold without boundary), and $N = S^{n-1}$, there is a unique solution to the general gradient-descent flow. Moreover, this solution is regular with the exception of a finite number of isolated points and the harmonic energy is decreasing in time. If the initial energy is small, the solution is completely regular and converges to a constant value. (These results actually hold for any compact N.) These uniqueness result was later extended to manifolds with smooth $\partial M \neq \emptyset$ and for weak solutions (Freire, 1995). Recapping, there is a unique weak solution to (11) (weak solutions defined in natural spaces, $H^{1,2}(M, N)$ or $W^{1,2}(M, N)$), and the set of possible singularities is finite. These solutions decrease the harmonic energy. The result is not completely true for M with dimension greater than 2, and this was investigated for example in Chen (1989). Global weak solutions exist for example for $N = S^{n-1}$, although there is no uniqueness for the general initial value problem (Coron, 1990). Results on the regularity of the solution, for a restricted suitable class of weak solutions, to the harmonic flow for high dimensional manifolds M into S^{n-1} have been recently reported (Chen et al., 1995; Feldman, 1994). In this case, it is assumed that the weak solutions hold a number of given energy constraints.

Singularities in 2D: If $N = S^1$, and the initial and boundary conditions are well behaved (smooth, finite energy), then the solution of the harmonic flow is regular. This is the case for example for smooth $2D$ image gradients and $2D$ optical flow.

Singularities in 3D: Unfortunately, for $n = 3$ in (11) (that is $N = S^2$, $3D$ vectors), smooth initial data can lead to singularities in finite time (Chang et al., 1992). Chang et al. showed examples where the flow (11), with initial data $I(x, y, 0) = I_0(x, y) \in C^1(D^2, S^2)$ (D^2 is the unit disk on the plane) and boundary conditions $I(x, y, t)|_{\partial D^2} = I_0|_{\partial D^2}$, develops singularities in finite time. The idea is to use as original data I_0 a function that covers S^2 more than once in a certain region. From the point of view of the harmonic energy, the solution is "giving up on" regularity in order to reduce energy.

Singularities topology: Since singularities can occur, it is then interesting to study them (Brezis et al., 1986; Hardt, 1997; Qing, 1995). For example, Brezis et al. studied the value of the harmonic energy when the singularities of the critical point are prescribed (the map is from R^3 to S^2 in this case).[5] Qing characterized the energy at the singularities. A recent review on the singularities of harmonic maps was prepared by Hardt (1997). (Singularities for more general energies are

studied for example in Pismen and Rubinstein (1991).) The results there reported can be used to characterize the behavior of the multiscale representation of high dimensional directions, although these results mainly address the shape of the harmonic map, that is, the critical point of the harmonic energy and not the flow. Of course, for the case of M being of dimension two, which corresponds to (11), we have Struwe's results mentioned above.

4. Anisotropic Diffusion

The picture becomes even more interesting for the case $1 \leq p < 2$. Now the gradient descent flow corresponding to (6), in the range $1 < p < 2$ (and formally for $p = 1$), with the constraint (7) is given by the set of coupled PDE's:

$$\frac{\partial I_i}{\partial t} = \operatorname{div}(\|\nabla I\|^{p-2}\nabla I_i) + I_i\|\nabla I\|^p, \quad 1 \leq i \leq n. \tag{12}$$

This system of coupled PDE's defines the anisotropic multiscale representation of $I(x, y, 0)$, which is used as initial datum to solve (11). In contrast with the isotropic case, now both terms in (12) are non-linear and include coupled components. Formally, we can also explicitly write the case $p = 1$, giving

$$\frac{\partial I_i}{\partial t} = \operatorname{div}\left(\frac{\nabla I_i}{\|\nabla I\|}\right) + I_i\|\nabla I\|, \quad 1 \leq i \leq n, \tag{13}$$

although the formal analysis and interpretation of this case is much more delicate than the description presented in the Appendix.

The case of $p \neq 2$ in (8) has been less studied in the literature. When M is a domain in $\mathbb{R}^m$, and $N = S^{n-1}$, the function $v(X) := \frac{X}{\|X\|}$, $X \in \mathbb{R}^m$, is a critical point of the energy for $p \in \{2, 3, \ldots, m-1\}$, for $p \in [m-1, m)$ (this interval includes the energy case that leads to (12)), and for $p \in [2, m - 2\sqrt{m-1}]$ (Hardt, 1997). For $n = 2$ and $p = 1$, the variational problem has also been investigated in Giaquinta et al. (1993), where the authors addressed, among other things, the correct spaces to perform the minimization (in the scalar case, $BV(\Omega, \mathbb{R})$ is used), and the existence of minimizers. Of course, we are more interested in the results for the flow (12), and not just in its corresponding energy. Some results exist for $1 < p < \infty$, $p \neq 2$, showing in a number of cases the existence of local solutions which are not smooth. To the best of our knowledge, the case of $1 \leq p < 2$, and in particular $p = 1$, has not been fully studied for the evolution equation, and this is part of our future plans.

Following the framework for robust anisotropic diffusion introduced in Black et al. (1998), we can generalize (5) and study problems of the form

$$\min_{I:\mathbb{R}^2 \to S^{n-1}} \int\int_{\Omega} \rho(\|\nabla I\|)\, dx\, dy, \tag{14}$$

where ρ is now a robust function like the Tukey biweight. Results on this approach will be reported elsewhere.

5. Examples

In this section we present a number of illustrative examples for the harmonic flows for $p = 2$ (isotropic) and $p = 1$ (anisotropic) presented above. These examples will mainly show that the proposed framework produces for directional data the same qualitative behavior that is well known and studied for scalar images. One of the advantages of directional diffusion is that, although advanced specialized numerical techniques to solve (5) and its corresponding gradient-descent flow, have been developed, e.g., Alouges (1991), as a first approximation we can basically use the algorithms developed for isotropic and anisotropic diffusion without the unit norm constraint to implement (11) and (12) (Cohen et al. 1987). Although, as stated before, these PDE's preserve the unit norm (that is, the solutions are vectors in S^{n-1}), numerical errors might violate the constraint (recent developments by Osher and Vese might solve this numerical problem (Osher and Vese, 1999)). Therefore, between every two steps of the numerical implementation of this equations we add a renormalization step (Cohen et al., 1987). Basically, a simple time-step iteration is used for (11), while for (12) we incorporate the edge capturing technique developed in Rudin et al. (1992) (we always use the maximal time step that ensures stability).

For the examples we show below, a number of visualization techniques are used (note that the visualization of vectors is an active research area in the graphics community):

1. Arrows. Drawing arrows indicating the vector direction is very illustrative, but can be done only for sparse images and they are not very informative for dense data like gradients or optical flow. Therefore, we use arrows either for toy examples or to show the behavior of the algorithm in local areas.

2. HSV color mapping. We use the HSV color map (applied to orientation) to visualize whole images of directions while being able to also illustrate details like small noise.
3. Line integral convolution (LIC) (Cabral and Leedom, 1993). LIC is based on locally integrating at each pixel the values of a random image. The integration is done in the line corresponding to the direction at the pixel. The LIC technique gives the general form of the flow, while the color map is useful to detect small noise in the direction (orientation) image.

All these visualization techniques are used for vectors in S^1. We also show examples for vectors in S^2. In this case, we consider these vectors as RGB vectors, and color is used to visualize the results.

Figure 1 shows a number of toy examples to illustrate the general ideas introduced in this paper. The first row shows, using LIC, an image with two regions having two different (2D) orientations on the left (original), followed by the results of isotropic diffusion for 200, 2000, and 8000 iterations (scale-space). Three different steps of the scale-space are shown in the next row using arrows. Note how the edge in the directional data is being smoothed out. The horizontal and vertical directions are being smoothed out to converge to the diagonal average. This is in contrast with the edges in the third row. This row shows the result of removing noise in the directional data. The original noisy image is shown first, followed by the results with isotropic and anisotropic smoothing. Note how the anisotropic flow gets rid of the noise (outliers) while preserving the rest of the data, while the isotropic flow also affects the data itself while removing the noise. Note that since the discrete theory developed in Perona (1998) applies only to small changes in orientation, theoretically it can not be applied to the images we have seen so far, all of them contain sharp discontinuities in the directional data. The last two rows of Fig. 1 deal with 3D directions. In this case, we interpret the vector as RGB coordinates, and use color to visualize them. First we show two steps in the scale space for the isotropic flow (original on the left). Then, the last row shows the original image followed by the results of isotropic and anisotropic diffusion. Note how the colors, and then the corresponding directions, get blurred with the isotropic flow, while the edges in direction (color) are well preserved with the anisotropic process. We can use this to process real color images. That is, we separate the color direction from the color magnitude, and use the harmonic flows to smooth the direction (we can use Alvarez et al. (1992) to smooth the magnitude). This will be exemplified below (other directional filters for color denoising, based on vectorial median filtering, can be found in Caselles and Sapiro (1998), Trahanias and Venetsanopoulos (1993) and Trahanias et al. (1996)).

Figure 2 shows results for optical flow.[6] The first figure on the first row shows a frame of the famous Yosemite movie. Next, in the same row, we show from left to right the original optical flow direction, the result of the isotropic flow, the result of the anisotropic flow, and the result of the isotropic flow for a large number of iterations. The HSV color map is used. In the next row, we use LIC to visualize again the three middle figures of the first row. In the third row, arrows are used to show a blown-up of the marked region corresponding to the isotropic flow for 20, 60, and 500 iterations. Note how the noise in the optical flow directions is removed.

Figure 3 deals with 90 degrees rotated gradient directions in a fingerprint image. After the raw data for the image is shown, we use the color map visualization technique to present a number of steps (scale-space) of the isotropic flow. This is followed by arrows for a blown-up of the marked region (last row, from left to right, original, 20 steps, and 200 steps respectively). Note in the arrows images how the noise and details (small scales) are removed, and progressively the "averaged" orientation for the fingerprint is obtained.

Figure 4 presents two examples for color images, that is, 3D directions defined on $\mathbb{R}^2$. Both columns show the original image, followed by the noisy image and the enhanced one. In the first column, noise is added only to the 3D RGB directions representing the chroma (the RGB vector normalized to a unit norm vector), while the magnitude of the vector (brightness) was kept untouched. The enhanced image was then obtained applying the proposed direction diffusion flow to the chroma, while keeping the original magnitude. This experiment shows that when the magnitude is preserved (or well reconstructed, see below), direction diffusion for chroma denoising produces an image practically indistinguishable from the original one. In the second column, the noise was added to the original image, resulting in both noisy chroma (direction) and brightness (magnitude) of the RGB vector. The directions are processed with the diffusion flow proposed in this paper, while the magnitude is processed with the scalar anisotropic flow in Black et al. (1998).

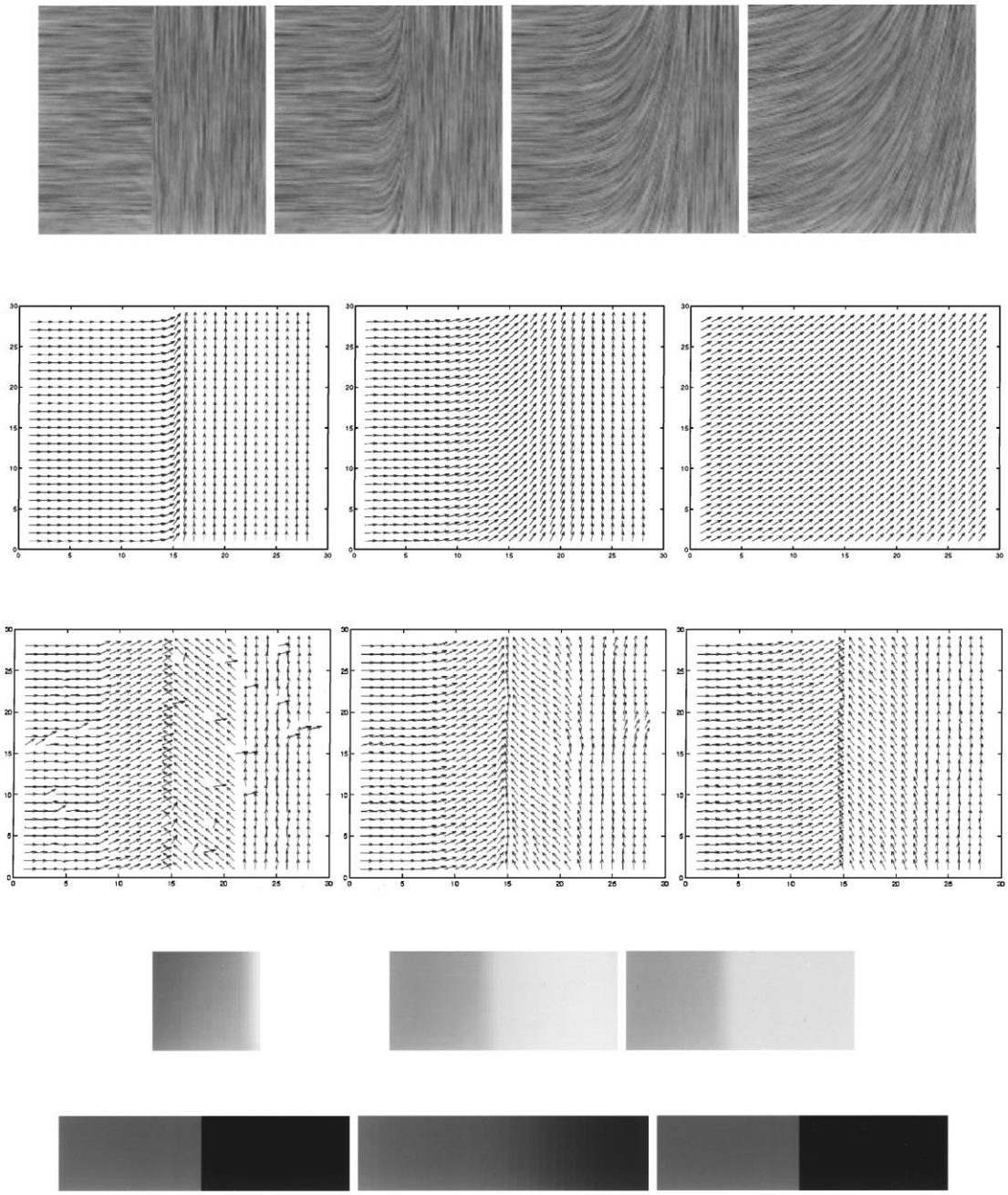

Figure 1. Toy examples illustrating the ideas in this paper. See text for details.

Isotropic and anisotropic direction diffusion flows on the chroma produce similar results as long as the magnitude is processed with an edge preserving denoising algorithm. See Tang et al. (1999) for additional examples, comparisons with the literature, and details on the applications of direction diffusion to color images.

6. Concluding Remarks

In this paper we have introduced a general framework for the multiscale analysis of directional data. The framework is based on the well studied area of harmonic maps. The technique applies to any dimension,

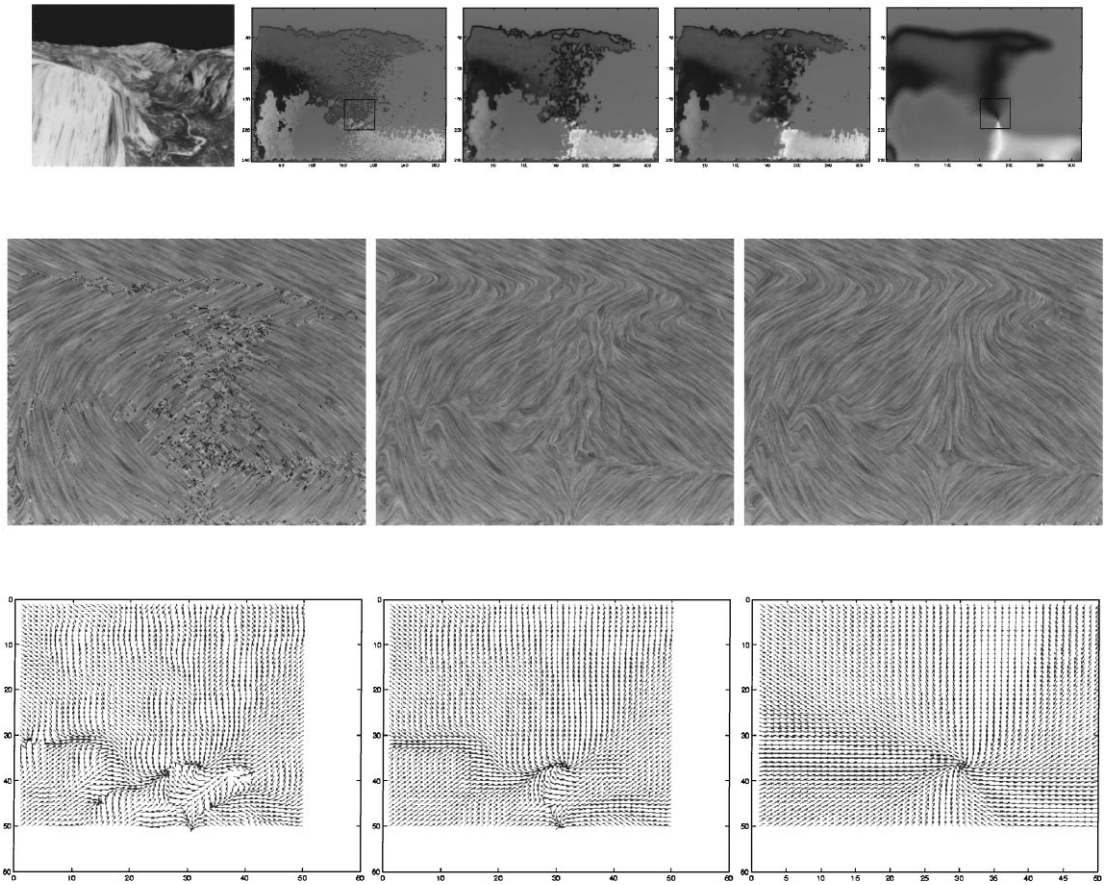

Figure 2. Optical flow example. See text for details.

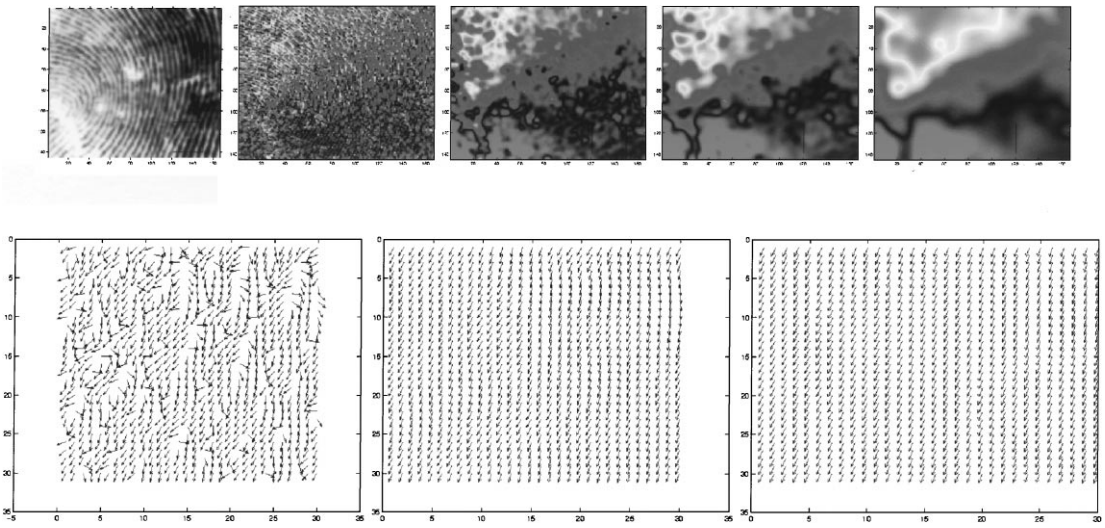

Figure 3. Gradient direction example. See text for details.

Figure 4. Denoising of a color image using 3D directional diffusion. See text for details.

smooth as well as non-smooth data, and both isotropic and anisotropic flows. The same framework can be applied to define isotropic and anisotropic diffusion flows on general data defined on general manifolds, not necessarily flat ones.

A number of questions remain open. First of all, we need to perform a complete analysis of the harmonic energy and gradient descent flow for $1 \leq p < 2$, the anisotropic case. We need at least results concerning with the existence and uniqueness of (weak) solutions.

From the practical point of view, it will be interesting to carry out a formal analysis that compares the results obtained from image denoising followed by direction computation (e.g., gradients) with those obtained while computing the directions in the noisy image and then smoothing them with the technique presented in this paper. In the case of color images, the best color space to apply the diffusion flows should be investigated as well. These questions are part of our current research. We are also planning on adding the harmonic map energy as a regularization constraint in ill-posed problems like optical flow computation. Last, as mentioned above, the use of the harmonic maps framework for diffusion on general manifolds (e.g., triangulated and implicit 3D surfaces), with a number of applications in graphics and medical imaging, will be reported elsewhere.

Appendix

We now derive the Euler-Lagrange equation for $p = 2$, Section 3. Similar computations can be used to derive the corresponding flows for $1 < p < +\infty$. The case $p = 1$ requires a different treatment (Anzellotti, 1985; Giaquinta et al., 1993), and Eq. (13) has to be seen as an evolution equation decreasing the energy E_1. The precise connection of (13) with the gradient descent of E_1 needs to be further analyzed.

Let Ω be a domain in $\mathbb{R}^2$ with smooth boundary and $n \geq 2$. As usual, $W^{1,2}(\Omega, \mathbb{R}^n)$ denotes the Sobolev space of functions $I(x_1, x_2) \in L^2(\Omega)$, whose distributional derivatives $\frac{\partial I}{\partial_{x_j}} \in L^2(\Omega)$, $j = 1, 2$. Let $W^{1,2}(\Omega, S^{n-1}) = \{I(x_1, x_2) \in W^{1,2}(\Omega, \mathbb{R}^n) : I(x_1, x_2) \in S^{n-1} a.e.\}$. Then it is known that functions $W^{1,2}(\Omega, S^{n-1})$ can be approximated by smooth maps (Bethuel and Zheng, 1988). If Ω is a square, the same result is true for $W^{1,2}(\Omega, S^1)$ (Bethuel and Zheng, 1988). We consider the energy functional $E : W^{1,2}(\Omega, S^{n-1}) \to \mathbb{R}$ given by the Dirichlet integral

$$E(I) = \int_\Omega \|\nabla I\|^2 \, dx, \quad I \in W^{1,2}(\Omega, S^{n-1}). \quad (15)$$

Now, let $I \in W^{1,2}(\Omega, S^{n-1})$ and let $\varphi \in C_o^\infty(\Omega, \mathbb{R}^n)$, the space of smooth functions in Ω vanishing outside a compact subset of Ω. Then we know that $\|I(x)\| = 1$ almost everywhere in Ω and, thus, for $|t|$ small enough $I + t\varphi$ is well defined and hence $I(t) := \frac{I+t\varphi}{\|I+t\varphi\|} \in W^{1,2}(\Omega, S^{n-1})$. Let us compute $\frac{d}{dt} E(I(t))|_{t=0}$. For that we observe that

$$\partial_{x_j} \|I + t\varphi\| = \frac{1}{\|I + t\varphi\|} \langle I + t\varphi, \partial_{x_j} I + t\partial_{x_j} \varphi \rangle. \quad (16)$$

Thus,

$$\partial_{x_j} I(t) = \frac{\partial_{x_j} I + t\partial_{x_j} \varphi}{\|I + t\varphi\|} - \frac{1}{\|I + t\varphi\|^3} \times \langle I + t\varphi, \partial_{x_j} I + t\partial_{x_j} \varphi \rangle (I + t\varphi).$$

On the other hand, observe that from the constraint $\langle I, I \rangle = 1$ a.e, it follows that $\langle I, \partial_{x_j} I \rangle = 0$. Since

$$\frac{1}{\|I + t\varphi\|} = 1 - t\langle I, \varphi \rangle + O(t^2),$$

where $O(t^2)$ means a quantity which is bounded by Ct^2, for some constant $C > 0$, then we may write

$$\partial_{x_j} I(t) = \partial_{x_j} I + tQ_j + O(t^2),$$

where

$$Q_j = -\langle \varphi, \partial_{x_j} I \rangle I - \langle I, \partial_{x_j} \varphi \rangle I + \partial_{x_i} \varphi - \langle I, \varphi \rangle \partial_{x_j} I.$$

Thus

$$\begin{aligned} &\frac{d}{dt} E(I(t)) \,|_{t=0} \\ &= 2 \int_\Omega \sum_{i=1}^2 \langle \partial_{x_j} I, Q_j \rangle \\ &= 2 \int_\Omega \sum_{j=1}^2 \langle \partial_{x_j} I, \partial_{x_j} \varphi \rangle - \langle I, \varphi \rangle \sum_{j=1}^2 \langle \partial_{x_j} I, \partial_{x_j} I \rangle. \end{aligned}$$

Since $\|\nabla I\|^2 = \sum_{j=1}^2 \langle \partial_{x_j} I, \partial_{x_j} I \rangle$, we may write the Euler-Lagrange equations corresponding to (15) as

$$\Delta I + I\|\nabla I\|^2 = 0 \quad \text{in } \Omega, \quad (17)$$

where ΔI denotes the Laplacian on each coordinate of I.

Acknowledgments

This work was originally motivated by the smoothing of vector-valued images, separating the vector into its direction and magnitude. GS thanks Prof. Robert

Kohn from the Courant Institute, NYU, for encouraging him to think again about filtering vectorial images. GS also wants to thank Prof. Kobi Rubinstein from the Technion, Israel Institute of Technology, for pointing out very relevant literature on harmonic maps, Prof. Stan Osher, Prof. Tony Chan, Dr. Luminita Vese and Prof. Jianhong Shen from UCLA for sharing their ideas on direction diffusion, Prof. David Heeger from Stanford University and Prof. Victoria Interrante from the University of Minnesota for pointing out references on vector visualization, Prof. Pietro Perona for helping with the color mapping visualization technique, and Brian Cabral and Casey Leedom, both from SGI, for the LIC software. Although this work was originally motivated by the smoothing of general vector-data, after making the connection with direction diffusion, Perona's work (Perona, 1998) was very influential and inspiring. The optical flow data was obtained using the software developed by Dr. Michael Black from Xerox PARC. The anonymous reviewers helped to improve the presentation of the paper. This work was partially supported by the TMR European project "Viscosity solutions and their applications," reference FMRX-CT98-0234, the European Network PAVR FMRXCT960036, a grant from the Office of Naval Research ONR-N00014-97-1-0509, the Office of Naval Research Young Investigator Award, the Presidential Early Career Awards for Scientists and Engineers (PECASE), a National Science Foundation CAREER Award, by the National Science Foundation Learning and Intelligent Systems Program (LIS), and NSF-IRI-9306155 (Geometry Driven Diffusion).

Notes

1. In this work we do not explicitly address the problem where the direction smoothing depends on other image attributes (see for example Lindeberg (1994)), the analysis is done intrinsically to the directional, unit norm, data. When other attributes are present, we process them separately or via couple PDE's, see the examples section and Tang et al. (1999). If needed, the unit norm constraint can be relaxed using a framework similar to the one here proposed.
2. Since the goal of this paper is to describe the general framework for direction diffusion, we will not add these type of constraints in the examples in Section 5. These constraints are normally closely tied to both the specific problem and the available information about the type of noise present in the image. In Chan and Shen (1999), data-terms are added.
3. For data like surface normals, principal directions, or simple gray values on 3D, M is a surface in 3D and the general flow (10) is used. This flow can be implemented using classical numerical techniques to compute ∇_M, Δ_M, $A_N(I)$ on triangulated surfaces, e.g., Angenent et al. (1998), Haker et al. (1999) and Hughes (1987). The harmonic maps framework can also be extended to data defined on *implicit* surfaces. Results on the multiscale analysis of directions and general data defined on surfaces instead of $\mathbb{R}$ will be reported in companion papers (the work on implicit surfaces is joint work with S. Osher).
4. The results below can also be obtained directly from the general Euler-Lagrange equations (9) and (10). The Laplace-Beltrami operator Δ_M and manifold gradient ∇_M become the regular Laplace and gradient respectively, since we are working on $\mathbb{R}^2$ (the same for $\mathbb{R}^n$). The second fundamental form $A_N(I)$ of the sphere (in any dimension) is I.
5. Perona suggested to look at this line of work to analyze the singularities of the orientation diffusion flow.
6. This simulated optical flow data was obtained from (Black and Anandan, 1993) (and down-loaded from M. Black's home page), stopping at early annealing stages to have enough noise for experimentation. This data is used here for illustration purposes only. Alternatively (see next section), we could include the harmonic energy as a regularization term inside the optical flow computation, that is, combined with the optical flow constraint.

References

Alouges, F. 1991. An energy decreasing algorithm for harmonic maps. In *Nematics*, J.M. Coron et al. (Eds.), Nato ASI Series, Kluwer Academic Publishers: Netherlands, pp. 1–13.

Alvarez, L., Lions, P.L., and Morel, J.M. 1992. Image selective smoothing and edge detection by nonlinear diffusion. *SIAM J. Numer. Anal.* 29:845–866.

Angenent, S., Haker, S., Tannenbaum, A., and Kikinis, R. 1998. Laplace-Beltrami operator and brain flattening. University of Minnesota ECE Report.

Anzellotti, G. 1985. The Euler equation for functionals with linear growth. *Transactions of the American Mathematical Society* 483–501.

Bethuel, F. and Zheng, X. 1988. Density of smooth functions between two manifolds in Sobolev spaces. *Journal of Functional Analysis* 80:60–75.

Black, M. and Anandan, P. 1993. A framework for the robust estimation of optical flow. In *Fourth International Conf. on Computer Vision*, Berlin, Germany, pp. 231–236.

Black, M., Sapiro, G., Marimont, D., and Heeger, D. 1998. Robust anisotropic diffusion. *IEEE Trans. Image Processing* 7(3):421–432.

Blomgren, P. and Chan, T. 1998. Color TV: Total variation methods for restoration of vector valued images. *IEEE Trans. Image Processing* 7:304–309.

Brezis, H., Coron, J.M., and Lieb, E.H. 1986. Harmonic maps with defects. *Communications in Mathematical Physics* 107:649–705.

Cabral, B. and Leedom, C. 1993. Imaging vector fields using line integral convolution. *ACM Computer Graphics (SIGGRAPH '93)* 27(4):263–272.

Caselles, V. and Sapiro, G. 1998. Vector median filters, morphology, and PDE's: Theoretical connections, ECE-University of Minnesota Technical Report. Also in Caselles, V., Sapiro, G., and Chung, D.H. Vector median filters, inf-sup operations, and coupled PDE's: Theoretical connections. *Journal of Mathematical Imaging and Vision*, pp. 109–120, April 2000.

Chan, T. and Shen, J. 1999. Variational restoration of non-flat image features: Models and algorithms. *UCLA CAM-TR 99-20*.

Chang, K.C., Ding, W.Y., and Ye, R. 1992. Finite-time blow-up of the heat flow of harmonic maps from surfaces. *J. Differential Geometry* 36:507–515.

Chen, Y. 1989. The weak solutions of the evolution problems of harmonic maps. *Math. Z.* 201:69–74.

Chen, Y., Hong, M.C., and Hungerbuhler, N. 1994. Heat flow of p-harmonic maps with values into spheres. *Math. Z.* 205:25–35.

Chen, Y., Li, J., and Lin, F.H. 1995. Partial regularity for weak heat flows into spheres. *Communications on Pure and Applied Mathematics* XLVIII:429–448.

Cohen, R., Hardt, R.M., Kinderlehrer, D., Lin, S.Y., and Luskin, M. 1987. In *Theory and Applications of Liquid Crystals*, J.L. Ericksen and D. Kinderlehrer (Eds.), Minimum energy configurations for liquid crystals: Computational results, IMA Volumes in Mathematics and its Applications. Springer-Verlag: New York, pp. 99–121.

Coron, J.M. 1990. Nonuniqueness for the heat flow of harmonic maps. *Ann. Inst. H. Poincaré, Analyse Non Linéaire* 7(4):335–344.

Coron, J.M. and Gulliver, R. 1989. Minimizing p-harmonic maps into spheres. *J. Reine Angew. Mathem.* 401:82–100.

Eck, M., DeRose, T., Duchamp, T., Hoppe, H., Lounsbery, M., and Stuetzle. W. 1995. Multiresolution analysis of arbitrary meshes. *Computer Graphics (SIGGRAPH '95 Proceedings)*, pp. 173–182.

Eells, J. and Lemarie, L. 1978. A report on harmonic maps. *Bull. London Math. Soc.* 10(1):1–68.

Eells, J. and Lemarie, L. 1988. Another report on harmonic maps. *Bull. London Math. Soc.* 20(5):385–524.

Eells, J. and Sampson, J.H. 1964. Harmonic mappings of Riemannian manifolds. *Am. J. Math.* 86:109–160.

Feldman, M. 1994. Partial regularity for harmonic maps of evolutions into spheres. *Comm. in Partial Differential Equations* 19:761–790.

Freire, A. 1995. Uniqueness for the harmonic map flow in two dimensions. *Calc. Var.* 3:95–105.

Giaquinta, M., Modica, G., and Soucek, J. 1993. Variational problems for maps of bounded variation with values in S^1. *Cal. Var.* 1:87–121.

Granlund, G.H. and Knutsson, H. 1995. *Signal Processing for Computer Vision*. Kluwer: Boston, MA.

Haker, S., Angenent, S., Tannenbaum, A., Kikinis, R., Sapiro, G., and Halle, M. 1999. Conformal surface parametrization for texture mapping. University of Minnesota IMA Preprint Series 1611.

Hardt, R.M. 1997. Singularities of harmonic maps. *Bulletin of the American Mathematical Society* 34(1):15–34.

Hardt, R.M. and Lin, F.H. 1987. Mappings minimizing the L^p norm of the gradient. *Communications on Pure and Applied Mathematics* XL:555–588.

Hughes, T. 1987. *The Finite Element Method*. Prentice-Hall: New Jersey.

Koenderink, J.J. 1984. The structure of images. *Biological Cybernetics* 50:363–370.

Lindeberg, T. 1994. *Scale-Space Theory in Computer Vision*. Kluwer: The Netherlands.

Osher, S. and Vese, L. 1999. Personal communication.

Pardo, A. and Sapiro, G. 1999. Vector probability diffusion. University of Minnesota, IMA preprint 1649, October 1999.

Perona, P. 1998. Orientation diffusion. *IEEE Trans. Image Processing* 7:457–467.

Perona, P. and Malik, J. 1990. Scale-space and edge detection using anisotropic diffusion. *IEEE Trans. Pattern. Anal. Machine Intell.* 12:629–639.

Pismen, L.M. and Rubinstein, J. 1991. Dynamics of defects. In *Nematics*, J.M. Coron et al. (Eds.), Nato ASI Series: Kluwer Academic Publishers: Netherlands, pp. 303–326.

Qing, J. 1995. On singularities of the heat flow for harmonic maps from surfaces into spheres. *Communications in Analysis and Geometry* 3(2):297–315.

Rudin, L.I. and Osher, S. 1994. Total variation based image restoration with free local constraints. *Proc. IEEE-ICIP* **I**, pp. 31–35, Austin, Texas.

Rudin, L.I., Osher, S., and Fatemi, E. 1992. Nonlinear total variation based noise removal algorithms. *Physica D* 60:259–268.

Sapiro, G. and Ringach, D. 1996. Anisotropic diffusion of multivalued images with applications to color filtering. *IEEE Trans. Image Processing* 5:1582–1586.

Sochen, N., Kimmel, R., and Malladi, R. 1998. A general framework for low level vision. *IEEE Trans. Image Processing* 7:310–318.

Struwe, M. 1985. On the evolution of harmonic mappings of Riemannian surfaces. *Comment. Math. Helvetici* 60:558–581.

Struwe, M. 1990. *Variational Methods*. Springer Verlag: New York.

Tang, B., Sapiro, G., and Caselles, V. 1999. Color image enhancement via chromaticity diffusion, pre-print.

Trahanias, P.E., Karakos, D., and Venetsanopoulos, A.N. 1996. Directional processing of color images: Theory and experimental results. *IEEE Trans. Image Processing* 5:868–880.

Trahanias, P.E. and Venetsanopoulos, A.N. 1993. Vector directional filters—A new class of multichannel image processing filters. *IEEE Trans. Image Processing* 2:528–534.

Weickert, J. 1996. Foundations and applications of nonlinear anisotropic diffusion filtering. *Zeitscgr. Angewandte Math. Mechan.* 76:283–286.

Weickert, J. 1999. Coherence-enhancing diffusion of color images. *Image and Vision Computing* 17:201–212.

Whitaker, R.T. and Gerig, G. 1983. Vector-valued diffusion. In *Geometry Driven Diffusion in Computer Vision*, Ber B. Haar Romeny, (Ed.). Kluwer: Boston, MA.

Witkin, A.P. 1983. Scale-space filtering. *Int. Joint. Conf. Artificial Intelligence* 2:1019–1021.

Yezzi, A. 1998. Modified curvature motion for image smoothing and enhancement. *IEEE Trans. Image Processing* 7:345–352.

You, Y.L., Xu, W., Tannenbaum, A., and Kaveh, M. 1996. Behavioral analysis of anisotropic diffusion in image processing. *IEEE Trans. Image Processing* 5:1539–1553.

Zhang, D. and Hebert, M. 1999. Harmonic maps and their applications in surface matching. *Proc. CVPR '99*. Colorado.